Acoustofluidic Separation of Microparticles: A Numerical Study

Nazemi Ashani, Mohsen; Bayareh, Morteza*+; Ghasemi, Behzad
Department of Mechanical Engineering, Shahrekord University, Shahrekord, I.R. IRAN

ABSTRACT: *In this study, two-dimensional simulations are performed to separate polystyrene (PS) and polymethyl methacrylate (PMMA) particles suspended in water using an acoustic field. The acoustic waves are generated by two aluminum interdigitated transducers (IDTs) over a piezoelectric substrate. The effect of input power, inlet flow rate, acoustic frequency, and distance between IDTs and channels on separation efficiency is evaluated by considering channel thickness. It is observed that the separation efficiency is enhanced by increasing acoustic frequency and input power. Also, as the inlet flow rate and distance between IDTs and channel decrease, the separation efficiency increases. The optimum values for input power, flow rate, frequency, and distance are 1.4 W, 0.2 mL/min, 5 MHz, and 75 µm, respectively, and a maximum separation of 88% is achieved.*

KEYWORDS: *Microfluidics; Acoustic field; Particle separation; Standing surface acoustic waves; Efficiency.*

INTRODUCTION

Microfluidic devices have been widely utilized due to their low cost, low energy consumption, and environmental compatibility, especially in biological applications [1-3]. These devices have been developed rapidly and used in many applications such as interdisciplinary science [4], chemical analysis [5], Lab-on-a-Chip (LOC) [6], etc. Microfluidic devices are divided into two groups: passive devices and active ones. In passive separation devices, particle separation is performed based on channel geometry [7]. Active devices use external forces, including electrical, optical, acoustic, and magnetic. For the case of active micromixing, *Xiong et al.* [8] employed a rhombic electroosmotic micromixer and reached a separation efficiency of 99% by applying an AC voltage of 10 V when the rhombic angle was 60°. Besides, *Feng et al.* [9] utilized Rubik's cube module to enhance the mixing efficiency of an electroosmotic micromixer. Also, some researchers appraised the impact of the magnetic force on the mixing process [10-11]. In the case of particle separation, *Shiriny and Bayareh* [12] performed numerical simulations to separate human breast and epithelial cervical cancer cells from the bloodstream using a spiral microchip. They also utilized a Halbach array of magnets to isolate blood cells [13] and inertial and magnetophoretic influences to separate PS particles [14]. They reached high purity of particle/cell separation for specific magnitudes of channel dimension, flow throughput, magnet distance from the channel, etc.

The acoustic-based separation approach proposes a completely different technique to isolate particles/cells with the advantages of simplicity and biocompatibility.

***** *To whom correspondence should be addressed.*
+ *E-mail: m.bayareh@sku.ac.ir*
1021-9986/2022/9/3064-3076 *13/$/6.03*

The sorting and isolation of particles/cells depend on their acoustic properties. Acoustic pressure wave causes particles or cells to migrate in a microchannel. Acoustic radiation force leads to the motion of particles toward the pressure nodes or antinodes [15]. Acoustic waves are divided into three types: Bulk Acoustic Wave (BAW), Surface Acoustic Wave (SAW), and Acoustic Plate Mode (APM) [16]. SAWs are a combination of longitudinal compression motion and transversal shear motion [17]. These waves are generated by InterDigital Transducers (IDTs) with comb-shaped electrodes. The SAW approach is classified into two types: Traveling SAW (TSAW) and Standing SAW (SSAW). TSAWs are generated when an IDT radiates a SAW and SSAWs are created when two IDTs radiate identical TSAWs. Acoustic streaming flow and acoustic radiation force are generated by TSAWs and SSAWs [18]. To manipulate particles, the acoustic streaming flow should be minimized [19]. Since SSAWs use two IDTs, the impact of acoustic streaming flow and their overall strength is reduced, leading to easier control of particle separation compared to TSAWs [20]. Besides, lower frequencies can be employed by SSAW-based acoustofluidic chips ($\sim$10 MHz) compared to TSAW-based ones ($\sim$100 MHz) [21].

Many researchers employed SSAWs to separate biological cells [22] or sort cells [23-25]. For instance, *Guo et al.* [22] used two IDTs for creating SAW to migrate particles toward the pressure nodes and showed that there is a good agreement between two-dimensional predictions and experimental observations. *Ma et al.* [23] used two IDTs and two sets of bandpass filtration to sort out PS particles with different diameters when the volume flow rate was varied between 1.5 and 4 μL/min. *Ren et al*. [24] used a pair of concentric circular-shaped IDTs (focused IDTs) to generate SSAWs for the sorting of 10-μm PS particles experimentally. They demonstrated that focused IDTs can generate stronger SAWs with higher sorting resolution in comparison with conventional IDTs, i.e. rectangular-shaped IDTs. *Li et al.* [25] used SSAWs to sort microfluidic water-in-oil droplets by changing the position of the pressure nodes. These efforts aimed to optimize the pressure field and acoustic radiation force to achieve high separation efficiency. Even though the variations of acoustic field amplitude have been investigated using different channel and IDT geometries, there are more required assessments to be performed. For example, the impact of channel thickness should be evaluated when inlet flow rate, acoustic frequency, and input power are varied.

The present study presents finite-element-based simulations to investigate the acoustic separation of PS and PMMA particles using SSAWs. The results obtained from the present numerical study are verified with experimental work. The impact of effective parameters is evaluated to control the generation of pressure nodes and antinodes as well as particle separation. In the present simulations, the influence of the thickness of the Polydimethylsiloxane (PDMS) channel is considered, meaning that current results can be used for practical applications.

THEORETICAL SECTION

Problem description

The geometry of the present study can be divided into three parts, i.e. InterDigital Transducers (IDTs), PDMS channel, and piezoelectric substrate, as shown in Fig. 1. Two InterDigital Transducers (IDTs) are placed on a piezoelectric substrate to generate acoustic waves. A PDMS channel is positioned between the IDTs. This channel has a rectangular cross-section of 160 μm x 100 μm depth and its length is 600 μm. The outlet channel has three branches, a middle one, and two tilted branches with an angle of 45°.

The aluminum IDTs are fabricated on a lithium niobate ($LiNbO_3$) piezoelectric substrate. The dimensions of IDTs are also described in Fig. 1. A voltage of $1.5V$ is applied to IDTs. CA creeping flow regime is assumed in the simulations; hence, the impact of inertia is neglected compared to the viscous effect. A no-slip boundary condition is imposed on the channel walls. Particles and fluid enter with a constant velocity of $V_{in} = 10^{-4}$ m/s. Besides, pressure outlet boundary condition is employed for channel outlets.

Governing equations

Acoustic frequency in a liquid medium creates pressure fluctuations, resulting in the application of radiation force on suspended particles. When the diameter of particles is much smaller than half of the wavelength, this force act on particles and moves them toward pressure nodes or antinodes [26-28]. A horizontal microchannel affected by acoustic waves is considered in the present study. The motion of microparticles in the fluid is described according to Newton's second law [29, 30]:

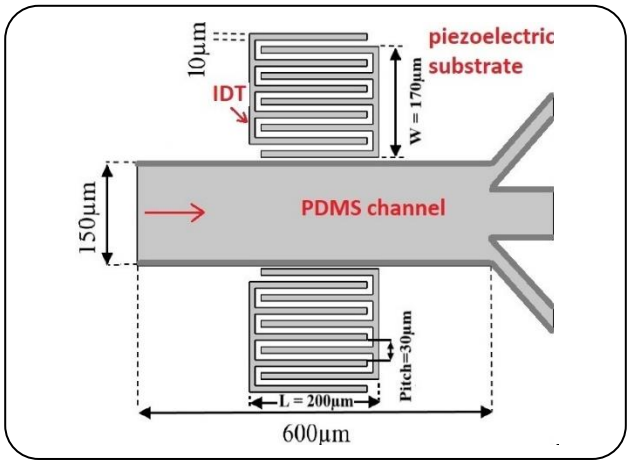

Fig. 1: Schematic of the present problem.

$$F = m_p \frac{du_p}{dt} \quad (1)$$

Where **F** is the total force applied to the particles, m_p is the particle mass, u_p is their velocity, and *t* is the time. The total force contains Drag force (F_D) and acoustic radiation force (F_{Rad}). For a spherical particle with diameter *d* moving with the velocity of u_p in the fluid flows with the velocity of u_f, the Drag force is [31-33]:

$$F_D = -3\pi\mu d(u_p - u_f) \quad (2)$$

Assuming incompressible fluid and neglecting gravity acceleration, the momentum equation is as follows:

$$\rho_f \frac{du_f}{dt} = -\nabla p + \mu\nabla^2 u_f \quad (3)$$

For spherical particles, the acoustic radiation force is:

$$F_{Rad} = -\nabla U_{Rad} \quad (4)$$

where U_{Rad} is acoustic potential energy [34]:

$$U_{Rad} = \frac{\pi}{6} d^3 \left(\frac{f_1}{2\rho c_f^2} \overline{p^2} - \frac{3f_2}{4} \rho \overline{u_i^2} \right) \quad (5)$$

where

$$f_1 = 1 - \frac{k_p}{k_f} \quad (6)$$

$$f_2 = \frac{2(\rho - \rho_f)}{2\rho + \rho_f} \quad (7)$$

where $c_f, k_p\ k_f, p, \rho$, and ρ_f are sound speed in the fluid, the compressibility of particles, compressibility of fluid, acoustic pressure, and density of particles and fluid, respectively. Besides, $\overline{p^2}$ and $\overline{\boldsymbol{u}_i^2}$ denote mean square pressure and incoming velocity amplitude, respectively. The direction of particles motion in the acoustic field depends on the sign of acoustic contrast factor, ϕ, that is calculated as follows:

$$\phi(\beta, \rho) = \frac{5\rho - 2\rho_f}{2\rho + \rho_f} - \frac{k_p}{k_f} \quad (8)$$

A positive contrast factor causes the particles to move towards pressure nodes. A negative one causes them to migrate towards the pressure antinodes. In the present simulations, the value of the contrast factor for PS and PMMA particles in the water medium is -0.28 and 1.16, respectively. Therefore, PS particles move towards pressure antinodes and PMMA ones migrate towards pressure nodes. Helmholtz equation should be solved to determine $\overline{p^2}$ and $\overline{\boldsymbol{u}_i^2}$. Since the effect of acoustic waves generated by the interaction between electric voltage and the piezoelectric substrate is considered, linear piezoelectric constitutive equations should be solved:

$$S = s_E T + e^t E \quad (9)$$

$$D = eS + \varepsilon_0 \varepsilon_r E \quad (10)$$

Where $D, S, T, E, \varepsilon_0, \varepsilon_r, s_E$, and e are charge density displacement, strain, stress, electric field, the permittivity of free space, relative permittivity matrix, compliance matrix, and piezoelectric coupling matrix, respectively. e^t denotes the transpose of matrix e. Besides, the acoustic pressure amplitude (p) is determined as follows:

$$p = \sqrt{\frac{PZ}{A}} \quad (11)$$

Where P, $Z = \rho_f \times c_f$, and A are input power, acoustic impedance, and SAW working area, respectively [35]. For the first set of simulations, the distance between IDTs and channel walls is assumed to be $75\mu m$. Since this value is equal to a quarter of a wavelength, one pressure node is formed at the centerline of the channel.

The finite element method and COMSOL Multiphysics software are employed to solve the governing equations. Navier-Stokes equations are solved using the finite element method and the P3+P2 scheme is selected to discretize the velocity and pressure. The P3+P2 approach considers the third-order derivative of the fluid velocity components and the second-order of pressure.

Table 1: Material properties of fluid and microparticles [36].

Property	PS	PMMA	Fluid
Diameter, µm	10	15	_
Density, kg/m^3	1050	1180	998
Sound speed, m/s	1260	2757	1481
Shear wave speed, m/s	1120	1400	-
Compressibility, Pa^{-1}	6.0 ×10^{-10}	1.3 ×10^{-12}	4.5 ×10^{-10}

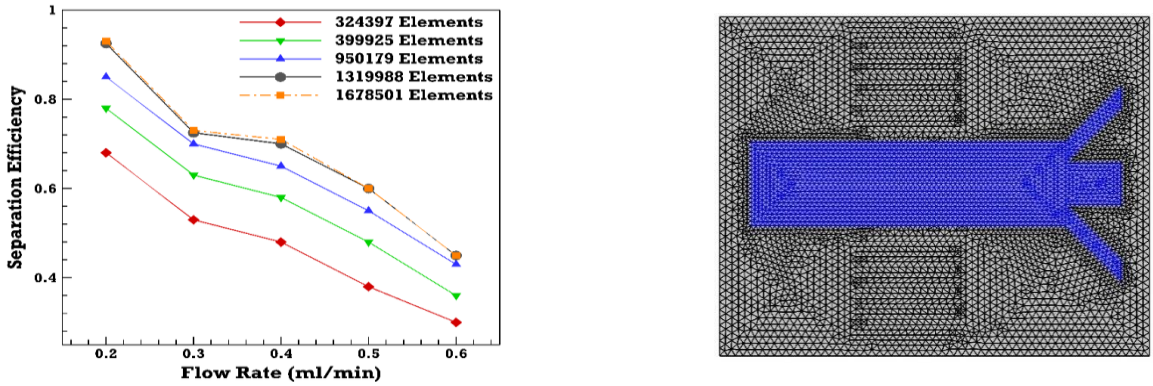

Fig. 2: (a) Separation efficiency for acoustic frequency of 13 MHz and different grid resolutions, and (b) the grid employed for current simulations.

The time step is 1 ms, and the relative tolerance convergence criterion is 10^{-5}. The Generalized Minimal Residual (GMRES) iterative solver is employed to solve the model. The GMRES solver generates a sequence of orthogonal vectors for asymmetric systems and the residual norm is computed with minimum iteration at every step. Electric potential and displacement fields are discretized by using quadratic and quadratic serendipity schemes, respectively. Numerical simulations are performed using 24-GB RAM, Intel (R) Core (TM) i7-6700K processor with a clock frequency of 4.00 GHz.

Grid study

A triangular mesh with a maximum size of $9\ \mu m$ and a minimum size of $1\mu m$ is generated for the channel and a triangular mesh with a maximum size of $15\mu m$ is used for substrate and IDTs. To find a sufficient number of grid points, the separation efficiency is calculated for an acoustic frequency of 13 MHz and different grid resolutions. The results are shown in Fig. 2a. As shown in this figure, by increasing the number of elements from 1319988 (gray line) to 1678501 (orange line), no noticeable change is observed in the value of separation efficiency (Fig. 2b). Thus, the computational grid with 1319988 elements is employed for further simulations. The physical properties of fluid and microparticles are presented in Table 1.

Validation

To verify the numerical simulation method, the separation efficiency is calculated for various flow rates according to the experimental data reported by *Petersson et al.* [37] (Fig. 3a). They used a 2 MHz frequency to separate lipid particles from erythrocytes in a microchannel with 350 µm width, 125 µm depth, and 24 mm length. Fig. 3a demonstrates good agreement between the numerical and experimental results so that the maximum error is less than 10%. In addition, the present results are verified with the numerical results of *Taatizadeh et al.* [38], who assessed the impact of some effective parameters such as the number of IDT fingers on separation efficiency using COMSOL Multiphysics software. Fig. 3b illustrates the amplitudes of normal acceleration across the channel achieved from the current work and those reported by *Taatizadeh et al.* [38], indicating

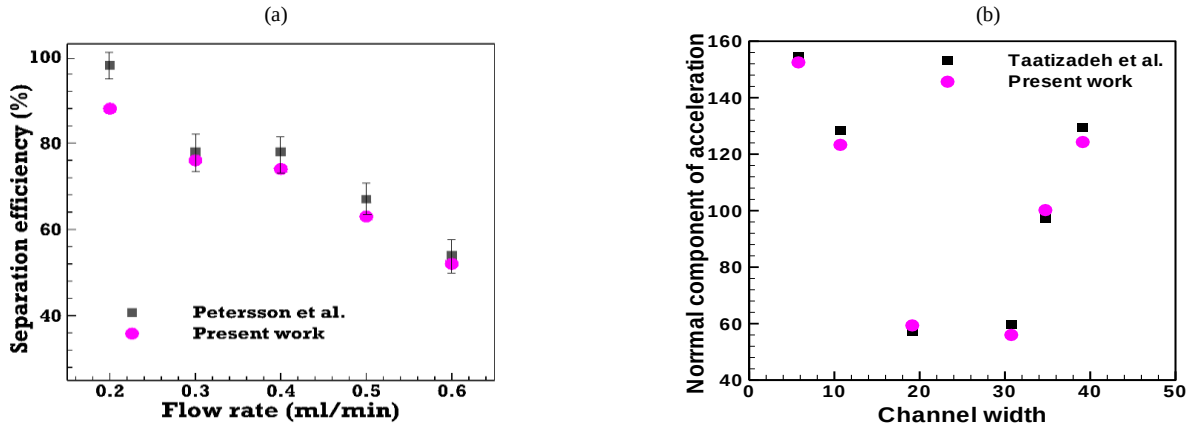

Fig. 3: (a) Separation efficiency versus flow rate when acoustic input power is 4 W, f = 5 MHz, D = 75μm, N_P = 4, and thickness of PDMS channel is 10μm, (b) the normal acceleration amplitude (μm/s2) across the microchannel width (μm) when N_P = 10.

good agreement between the results. *Taatizadeh et al.* [38] revealed that N_p = 20, 60, and 80 can provide the maximum amounts of normal acceleration. The influence of the number of IDT fingers is discussed in the Section "Effect of the number of IDT fingers".

RESULTS AND DISCUSSION

In the present paper, the effect of the power of IDTs, the acoustic frequency, flow rate, distance of IDTs from the channel wall, the number of IDT fingers, and the thickness of the PDMS channel during the separation process is investigated.

Effect of input power

In this section, the impact of input power on separation efficiency is evaluated for a constant operating frequency of 5 MHz and flow rate of 0.2 μl/min. The propagation of SSAW in the piezoelectric substrate leads to the creation of the electrical field in $LiNbO_3$ due to the coupling of the electrical field and mechanical strain. Hence, the piezoelectric substrate becomes an electrode. Fig. 4 demonstrates that the separation efficiency is enhanced with the input power. According to Eq. 10, an increase in the input power results in an enhancement in the acoustic pressure, leading to an increase in the acoustic radiation force. Thus, as the input power increases, the particles are affected more by the radiation force, migrating toward pressure nodes and antinodes more quickly. It should be pointed out that as the input power is enhanced, acoustic radiation force leads to Joule heating, formation of bubbles, and accumulation of microparticles, resulting in

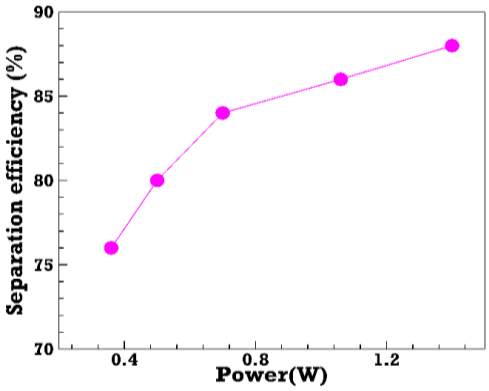

Fig. 4: Separation efficiency for various values of input power when the volume flow rate is 0.2 mL/min, f = 5 MHz, D = 75μm, N_P = 4, and the thickness of the PDMS channel is 10μm.

the creation of disturbance in chip operation practically [38]. Fig. 4 demonstrates that the majority of particles is separated (separation efficiency is about 88%) when the input power is 1.5 W. Numerical and experimental investigation of [38] revealed that the migration of particles is not affected by input power when the voltage is greater than 15 V.

Effect of inlet flow rate

The influence of the inlet flow rate on the separation efficiency is considered in Fig. 5 when the frequency and input power are kept constant at 5 MHz and 1.4 W, respectively. As the volume flow rate changes from 0.2 to 0.6 mL/min, separation efficiency varies from 88% to 44%. *Petersson et al.* [37] also demonstrated that higher

separation efficiencies can be obtained at lower flow rates. For the lower flow rates, particles are exposed to the acoustic field for a longer time. Hence, stronger acoustic force is applied to the particles, leading to larger lateral migration. It can be concluded that the separation efficiency is a decreasing function of flow rate. This result is important when there is a solution containing a high concentration of particles, such as blood and cancer cells. Therefore, in the solutions with a high volume fraction of suspending particles, some techniques, such as the use of sheath flow, variation of IDT configuration, and changing of acoustic frequency can be employed to achieve high separation efficiency.

Effect of acoustic frequency

In Fig. 6, the variation of separation efficiency is shown when acoustic field frequency is changed. An increment in the frequency causes an enhancement in the separation efficiency. As the frequency is increased, the wavelength is reduced:

$$\lambda = \frac{c_f}{f} \qquad (12)$$

where f is the acoustic frequency, c_f is the sound speed, and λ is the wavelength. By increasing the frequency, the wavelength is decreased, causing the pressure nodes and antinodes to change across the channel. The increase in the frequency leads to the creation of more pressure nodes, resulting in higher separation efficiency. Fig. 7 demonstrates the impact of acoustic frequency on the variation of pressure nodes and antinodes.

Effect of distance between IDTs and channel

The distance between IDTs and channel wall (D) affects the location of pressure nodes and antinodes. First, the distance between IDTs and channel is assumed to be 75 µm that is equal to a quarter of the wavelength. Therefore, a pressure node is formed at the center of the channel, and two pressure antinodes are formed near the walls (Fig. 8a). Figs. 8b and 8c reveal the location of pressure nodes and antinodes for D = 50 µm and 25µm, respectively. It is found that the pressure antinode is located closer to the channel centerline when D = 25 µm in comparison with the case in which D = 50 µm. According to Eq. 11, when D = 0 µm, pressure antinodes are formed in the middle of the channel (Fig. 8d). Fig. 9 shows the variation of separation efficiency in terms of the

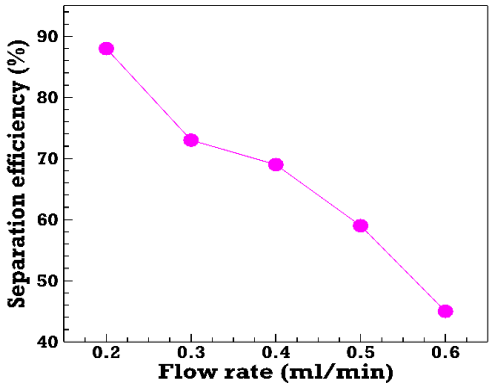

Fig. 5: Separation efficiency as a function of volume flow rate when input power is 1.4 W, f = 5 MHz, D = 75µm, N_P = 4, and thickness of PDMS channel is 10µm.

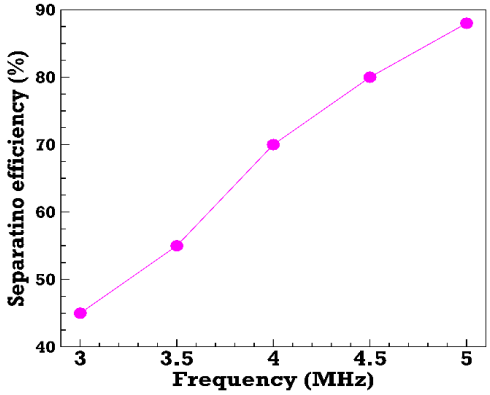

Fig. 6: Separation efficiency as a function of acoustic frequency when the volume flow rate is 0.2 mL/min, input power is 1.4 W, D = 75µm, N_P = 4, and thickness of PDMS channel is 10µm.

distance between IDTs and channel. Since the PS particles move toward pressure antinodes, the best location of IDTs is D = 75 µm, where two pressure antinodes are located at the channel walls. Hence, these particles can exit from two side outlets.

Effect of the number of IDT fingers

In an acoustic field, the energy of waves depends on the input voltage. By increasing input power (input voltage), the pressure of waves is enhanced. One way to increase input power is to enhance the number of IDT fingers (N_p). In other words, as N_p of IDTs is increased, the coupling coefficient of the piezoelectric substrate becomes greater, resulting in an enhancement in the value of energy that is

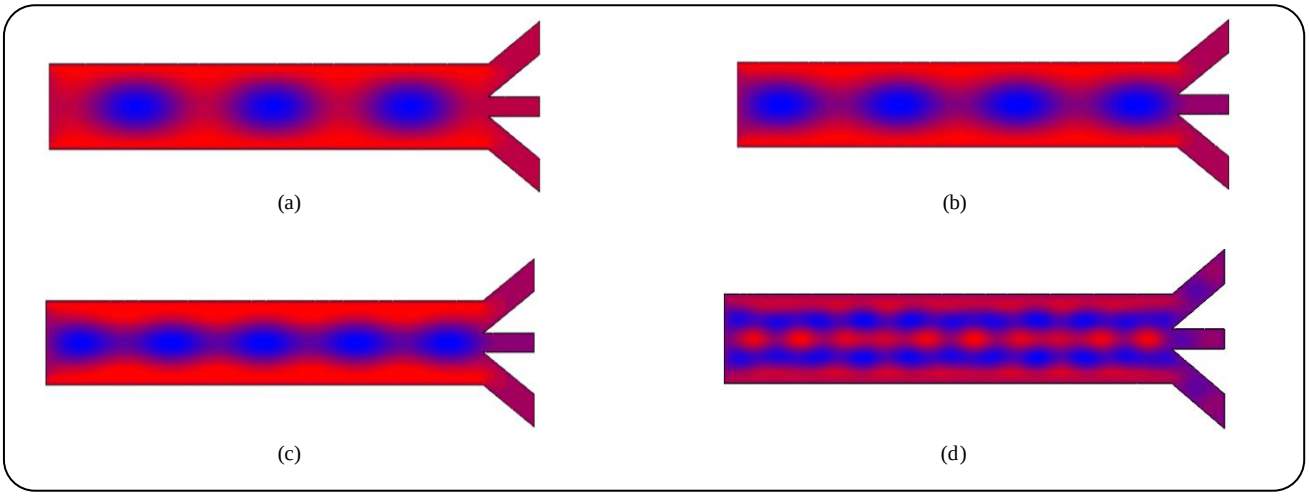

Fig. 7: Generation of pressure nodes when volume flow rate is 0.2 mL/min, input power is 1.4 W, D = 75µm, N_P = 4, thickness of PDMS channel is 10µm, and (a) f = 3 MHz, (b) f = 4 MHz, (c) f = 5 MHz, and (d) f = 10 MHz.

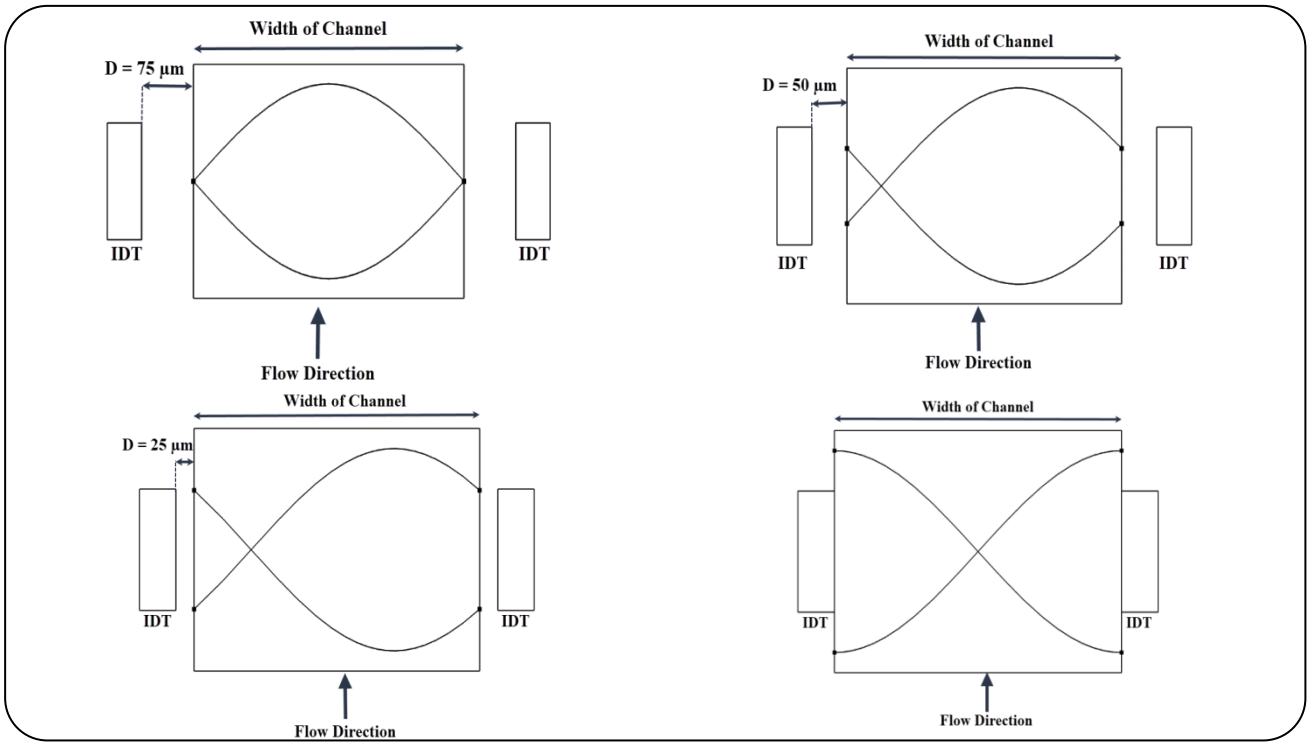

Fig. 8: Effect of the distance between IDTs and channel walls on the location of pressure nodes and antinodes when the volume flow rate is 0.2 mL/min, input power is 1.4W, f = 5 MHz, N_P = 4, and thickness of PDMS channel is 10µm.

transduced in the transducers. The number of fingers of IDT affects the acoustic pressure of waves and piezoelectricity properties. When the number of fingers of IDT is increased, the acoustic pressure is enhanced; however, there is a limitation in the substrate area [32]. Besides, it was found that there is a critical value for N_p so that the acceleration amplitude and energy transmission are weakened when $N_p > N_{p,\ critical}$. *Taatizadeh et al.* [38] reported that N_p = 20, 50, and 80 provides the most separation efficiency. Fig. 10 shows that the separation efficiency is an increasing function of N_p. For instance, separation efficiency is 75% and 95% when N_p = 2 and 8, respectively. It is expected that the ascending trend is retained even for N_p = 25.

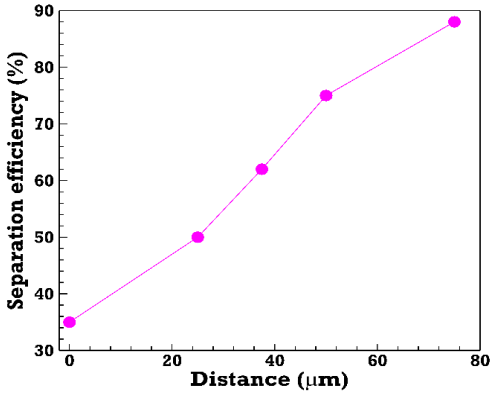

Fig. 9: Separation efficiency as a function of the distance between IDTs and channel wall when the volume flow rate is 0.2 mL/min, input power is 1.4 W, f = 5 MHz, N_p = 4, and thickness of PDMS channel is 10μm.

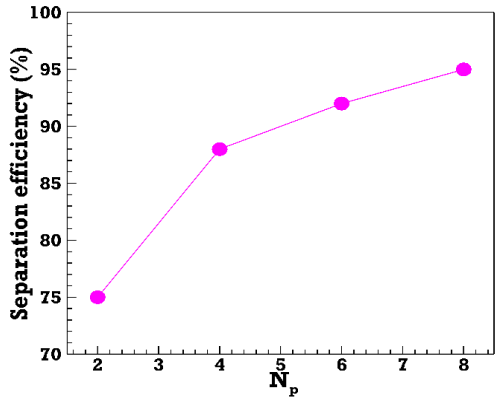

Fig. 10: Separation efficiency versus the number of IDT fingers when the volume flow rate is 0.2 mL/min, input power is 1.4 W, f = 5 MHz, D =75μm, and thickness of PDMS channel is 10μm.

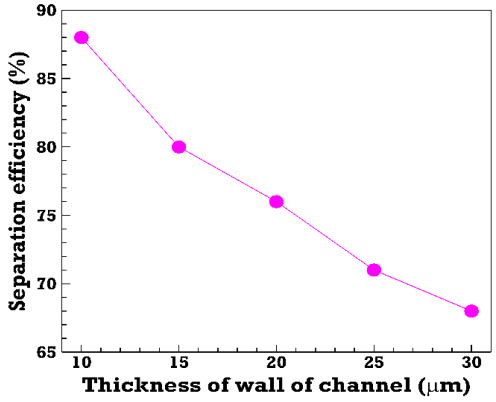

Fig. 11: Separation efficiency as a function of channel wall thickness when the volume flow rate is 0.2 mL/min, input power is 1.4 W, f = 5 MHz, D = 75 μm, and N_p= 4.

Effects of PDMS channel thickness

The acoustic waves created by IDTs collide with the PDMS channel walls and lose some of their energy. Therefore, an increase in the channel thickness results in a reduction in the acoustic pressure and separation efficiency. It has been shown that the position of pressure nodes and pressure antinodes depends on the channel width [38]. In the case of SSW, one and two pressure nodes are formed when the microchannel width is equal to $\lambda_{SSW}/2$ and λ_{SSW}, respectively. It can be concluded that the number of pressure nodes is enhanced with the channel width. It is expected that as the PDMS's thickness is reduced, the acoustic radiation force becomes stronger when input power and acoustic frequency are kept constant. This is due to the smaller dissipation of acoustic energy into the PDMS domain. When SSAWs reach the PDMS, they are distributed in PDMS, leading to a reduction in the normal component of the displacement at the surface of the piezoelectric substrate before reaching the microchannel and fluid domain. The acoustic pressure is reduced with the PDMS's width [38]. The separation efficiency versus the thickness of the PDMS is shown in Fig. 11. The values of effective parameters are as follows: input power is 1.4 W, f = 5 MHz, D = 75μm, and N_p= 4. The PDMS's width varies from 10 to 30 μm. When PDMS's thickness = 10 μm that is equal to $1/30$ of the wavelength, the strong acoustic pressure in the middle of the microchannel leads to that almost all PS particles move toward pressure antinodes. Hence, these particles exit from the side outlets, and the separation efficiency is relatively high. It should be pointed out that the thickness of the PDMS channel is limited by fabrication techniques such as soft lithography, 3D printing, etc.

Particle tracing

In the present simulations, particles with diameters of 10 μm (PS particles) and 15 μm (PMMA particles) are separated due to the application of the acoustic field. In general, two forces act upon particles, including acoustic radiation force and drag force. Eq. 4 expresses that the acoustic radiation force is proportional to acoustic potential energy. Eq. 5 shows that $U_{Rad} \sim d^3$; thus, as the particle diameter increases, the magnitude of $\boldsymbol{F}_{Rad}$ is enhanced. Therefore, the particles with larger diameters (PMMA particles) migrate towards the channel centerline. In the absence of an acoustic field, macro and

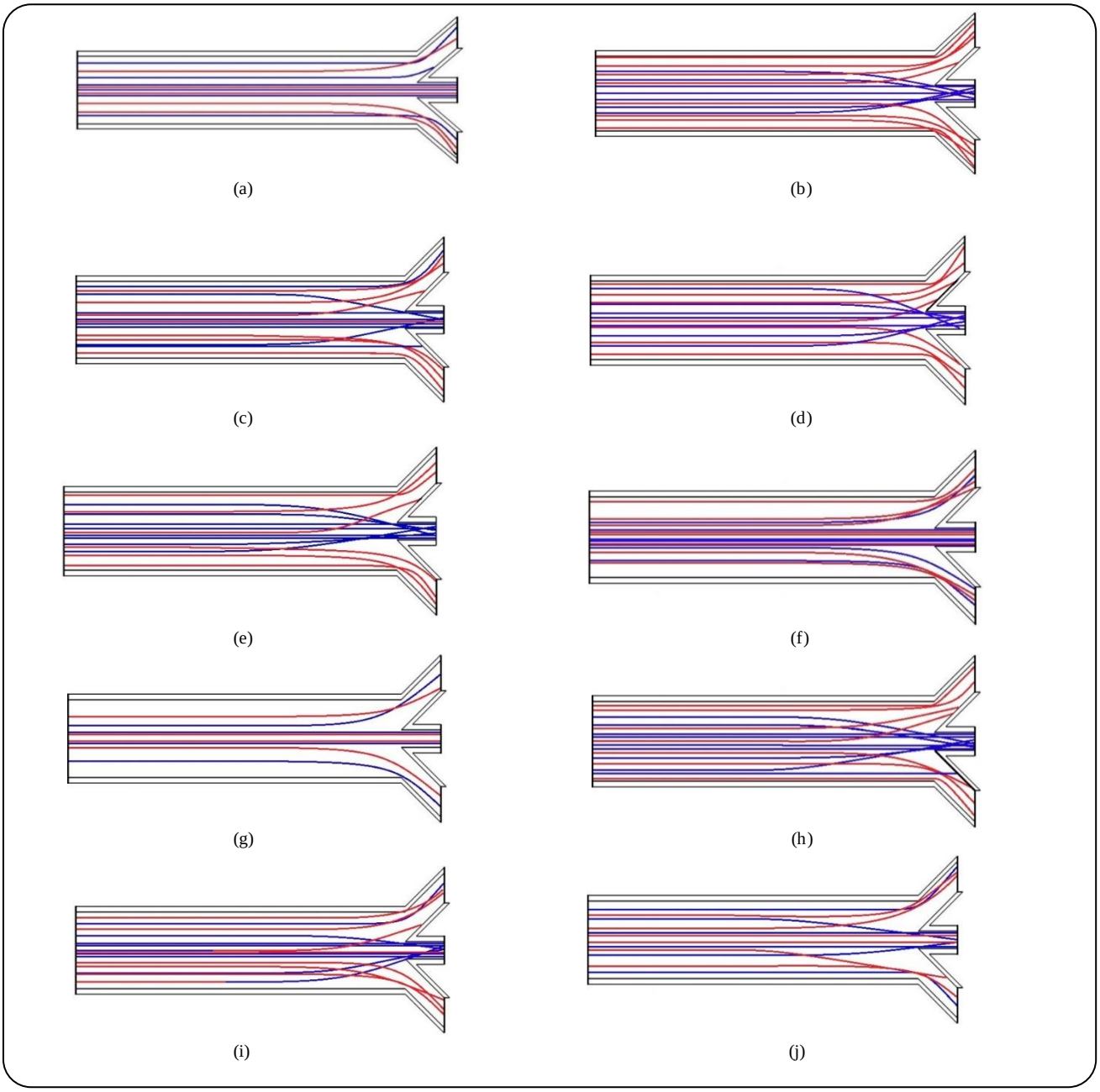

Fig. 12: Particle trajectories for the case where N_p = 4 and (a) D = 0.25 µm, volume flow rate = 0.2 mL/min, input power = 1.4 W, and f = 3 MHz, (b) D = 0.75µm, volume flow rate = 0.2 mL/min, input power = 1.4 W, and f = 5 MHz, (c) input power = 0.36 W, volume flow rate = 0.2 mL/min, f = 5 MHz, and D = 75µm, (d) input power = 1.4 W, volume flow rate = 0.2 mL/min, f = 5 MHz, and D = 75µm, (e) inlet flow rate = 0.2 mL/min, input power = 1.4 W, f = 5 MHz, and D = 75µm, (f) inlet flow rate = 0.6 mL/min, input power = 1.4 W, f = 5 MHz, and D = 75µm, (g) f = 3 MHz, volume flow rate = 0.2 mL/min, input power = 1.4 W, and D = 75µm, (h)) f = 5 MHz, volume flow rate = 0.2 mL/min, input power = 1.4 W, and D = 75µm, (i) PDMS thickness = 10 µm, volume flow rate = 0.2 mL/min, input power = 1.4 W, f = 5 MHz, and D = 75µm, and (j) PDMS thickness = 30 µm, volume flow rate = 0.2 mL/min, input power = 1.4 W, f = 5 MHz, and D = 75µm.

microparticles move towards a position between the channel centerline and the wall due to wall repulsion and velocity distribution [39-40]. Hence, it is expected that these particles exit from the side outlets with no separation.

Fig. 12 illustrates the particle trajectories for different values of acoustic frequency, flow rate, input power, number of IDT fingers, and PDMS thickness. The 'Particle Tracing' module in the COMSOL Multiphysics software

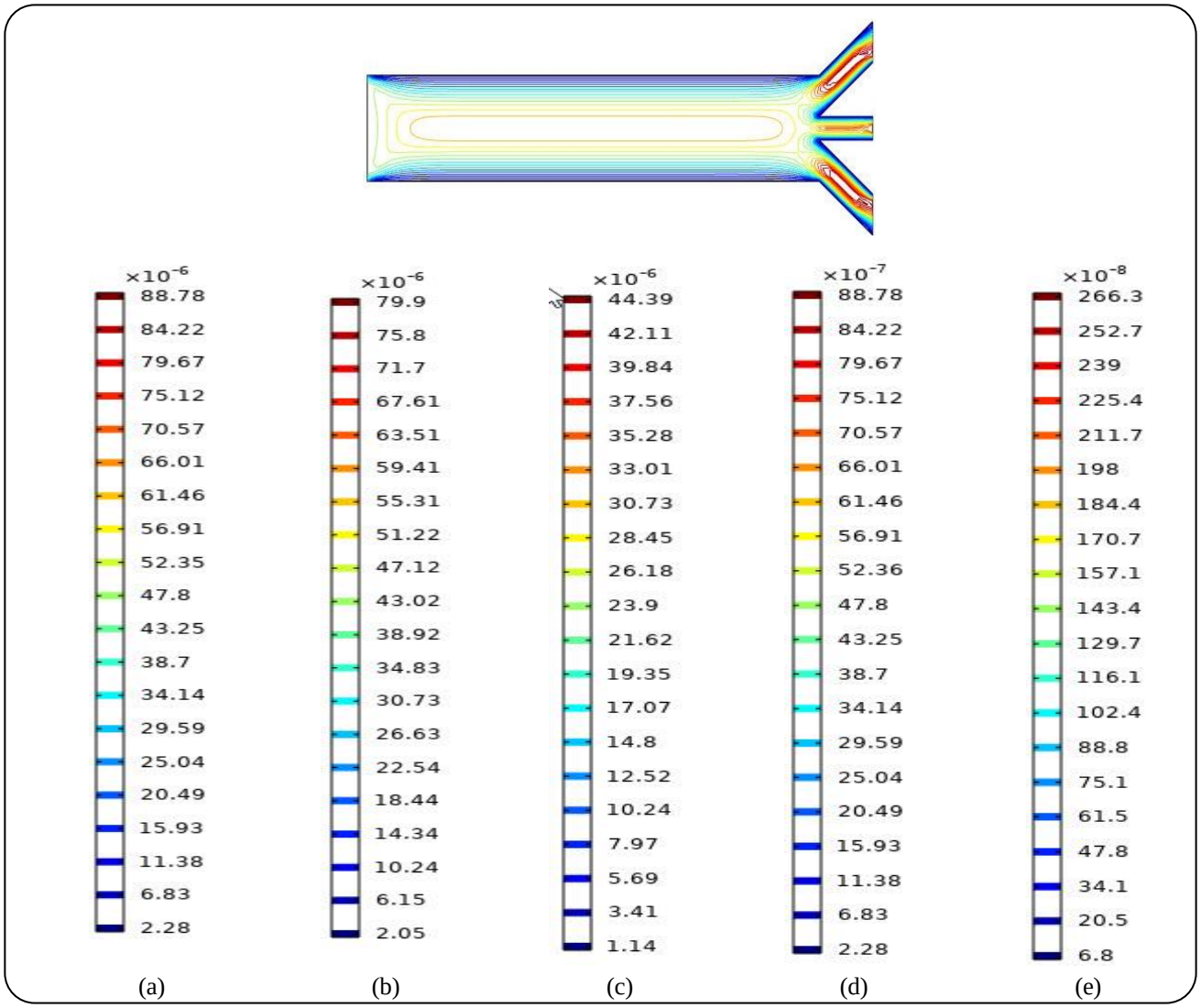

Fig. 13: Velocity contours for the case where $N_P = 4$ and (a) D = 0.25µm, volume flow rate = 0.2 mL/min, input power = 1.4 W, and f = 5 MHz, (b) D = 0.75µm, volume flow rate = 0.2 mL/min, input power = 1.4 W, and f = 3 MHz, (c) PDMS thickness = 10 µm, volume flow rate = 0.2 mL/min, input power = 1.4 W, f = 5 MHz, (d) PDMS thickness = 30 µm, volume flow rate = 0.2 mL/min, input power = 1.4 W, f = 5 MHz, and D = 75µm, and € input power = 0.36 W, volume flow rate = 0.2 mL/min, f = 5 MHz, and D = 75µm.

is employed to estimate the particle trajectories. This figure shows that for D = 0.25µm, the acoustic radiation force is so small that particles' motion is not affected by this force. Hence, PS and PMMA particles exit the channel through the middle and side outlets. For D = 0.75µm, the acoustic radiation force is so large that most of PMMA particles are forced to the channel center and exit through the middle outlet. PS particles, however, migrate toward sidewalls and exit from side outlets. These explanations are valid when acoustic frequency, input power, inlet flow rate, and PDMS thickness are changed. It can be concluded that effective parameters should be optimized to separate or sort microparticles in the presence of acoustic radiation force. Eventually, the modeled fluid velocity distribution in the whole continuous microfluidic channel has been plotted to better understand the fluid flow field (Fig. 13). It should be pointed out that the qualitative velocity distribution is approximately the same when effective parameters are changed. However, the variation range of velocity is different for various conditions.

CONCLUSIONS

Since the physical properties of cells are considered by acoustic-based separation techniques, acoustofluidic

devices are utilized to sort or isolate bio-cells suspended in microfluidics. The present work presented two-dimensional simulations for isolating PS and PMMA particles suspended in water using an acoustic field using the finite element method. The effect of input power, inlet flow rate, acoustic frequency, and distance between IDTs and channels on separation efficiency was investigated. It was observed that as the input power is increased, the separation efficiency is enhanced so that the maximum separation efficiency of 88% can be achieved when the input power is 1.4 W. The results demonstrated that separation efficiency is a decreasing function of volume flow rate and an ascending function of acoustic frequency. It was shown that the distance between IDTs and the channel wall affects the separation efficiency significantly. When the frequency was 5 MHz and the distance between IDTs and the channel wall was 75μm, a pressure node was formed at the center of the channel, leading to maximum separation efficiency because PMMA particles move toward the pressure node and PS ones migrate toward pressure antinodes. Besides, it was found that an increase in the number of fingers of IDT results in an increment in the separation efficiency. It should be pointed out that the impact of the thickness of the PDMS channel was considered in the present work; hence, current results can be used for practical applications. The influences of the non-Newtonian continuous phase, for instance, viscoelastic microfluidics, on acoustic-based particle/cell separation can be evaluated in future investigations numerically and experimentally. Besides, the combined effects of inertial and acoustic forces can be utilized to propose a high-throughput separation device.

Received : Aug. 10, 2021 ; Accepted : Nov. 1, 2021

REFERENCES

[1] Sajeesh P., Sen A.K., Particle Separation and Sorting in Microfluidic Devices: A Review, *Microfluid Nanofluid*, **17**: 1–52 (2014).

[2] Kashaninejad N., Nikmaneshi M.R., Moghadas H., Oskouei A.K., Rismanian M., Barisam M., Saidi M.S., Firoozabadi B., Organ-Tumor-on-a-Chip for Chemosensitivity Assay: A Critical Review, *Micromachines*, **7**: 130 (2016).

[3] Fathi F., Rahbarghazi R., Rashidi M.R., Label-free Biosensors in the Field of Stem Cell Biology, *Biosensors and Bioelectronic*, **101**: 188-198 (2017).

[4] Staufer O., Antona S., Zhang D., Csatari J., Schroter M., Janiesch J.W., Fabritz S., Berger I., Platzman I., Microfluidic Production and Characterization of Biofunctionalized Giant Unilamellar Vesicles for Targeted Intracellular Cargo Delivery, *Biomaterials*, **264**: 120203 (2021).

[5] Torkaman R., Torab-Mostaedi M., Safdari J., Moosavian S.M.A., Asadollahzadeh M., Mass Transfer Coefficients in Pulsed Column for Separation of Samarium and Gadolinium, *Iranian Journal of Chemistry and Chemical Engineering (IJCCE)*, **36**: 145–158 (2017).

[6] Li Q., Zhou S., Zhang T., Zheng B., Tang H., Bioinspired Sensor Chip for Detection of miRNA-21 Based on Photonic Crystals Assisted Cyclic Enzymatic Amplification Method, *Biosensors and Bioelectronics*, **150**: 111866 (2020).

[7] Bayareh M., An Updated Review on Particle Separation in Passive Microfluidic Devices, *Chemical Engineering and Processing-Process Intensification*, **153**: 107984 (2020).

[8] Xiong S., Chen X., Chen H., Chen Y., Zhang W., Numerical Study on an Electroosmotic Micromixer with Rhombic Structure, *Journal of Dispersion Science and Technology*, 1–7 (2020).

[9] Feng Q., Chen X., Wang X., Yu X., Zeng X., Ma Y., Wang Q., Numerical Simulation of a Three Dimensional Electroosmotic Micromixer with a Flexible and Controllable Rubik's Cube Module, *International Communications in Heat and Mass Transfer*, **127**: 105482 (2021).

[10] Bayareh, M., Ashani M.N., Usefian A., Active and Passive Micromixers: A Comprehensive Review. *Chemical Engineering and Processing-Process Intensification*, **147**: 107771 (2020).

[11] Usefian A., Bayareh M., Shateri A., Taheri N., Numerical Study of Electro-Osmotic Micro-Mixing of Newtonian and Non-Newtonian Fluids, *Journal of the Brazilian Society of Mechanical Sciences and Engineering*, **41(5)**: 1-10 (2019).

[12] Shiriny A., Bayareh M., Inertial Focusing of CTCs in a Novel Spiral Microchannel, *Chemical Engineering Science*, **229**: 116102 (2021).

[13] Shiriny A., Bayareh M., On Magnetophoretic Separation of Blood Cells Using Halbach Array of Magnets, *Meccanica*, **55**: 1905-1916 (2020).

[14] Shiriny A., Bayareh M., Ahmadi Nadooshan A., Combination of Inertial Focusing and Magnetophoretic Separation in a Novel Microdevice, *Korean Journal of Chemical Engineering*, **38**: 1686-1702 (2021).

[15] Shi J., Huang H., Stratton Z., Huang Y., Huang T.J., Continuous Particle Separation in a Microfluidic Channel via Standing Surface Acoustic Waves (SSAW), *Lab. on a Chip.*, **24**: 3354–3359 (2009).

[16] Glynne-Jones P., Boltryk R.J., Harris N.R., Cranny A.W., Hill M., Mode-switching: A New Technique for Electronically Varying the Agglomeration Position in an Acoustic Particle Manipulator, *Ultrasonics*, **50**: 68–75 (2010).

[17] Destgeer G., Im S., Ha B.H., Ansari M.A., Adjustable, Rapidly Switching Microfluidic Gradient Generation Using Focused Travelling Surface Acoustic Waves, *Applied Physics Letters*, **104**: 023506 (2014).

[18] Oseev A., Lucklum R., Zubtsov M., Schmidt M.P., SAW based Phononic Crystal Liquid Sensor-Periodic Microfluidic Channels Approach, IEEE International Ultrasonics Symposium (IUS). INSPEC Accession Number: 16429142, Electronic ISSN: 1948-5727 (2016).

[19] Wu C.H., Yang C.H., Guided Waves Propagating in a Bi-layer System Consisting of a Piezoelectric Plate and a Dielectric Fluid Layer, *IEEE Transactions on Ultrasonics, Ferroelectrics, and Frequency Control*, **58**: 1612-1618 (2011).

[20] Alzuaga S., Ballandras S., Bastien F., Daniau W., Gauthier-Manuel B., Manceau J.F., Cretin B., Vairac P., Laude V., Khelif A., Duhamel R., A Large Scale XY Positioning and Localisation System of Liquid Droplet Using SAW on $LiNbO_3$, *IEEE Ultrasonics Symposium*, **32**: 1790-1793 (2003).

[21] Wang T., Ke M., Qiu C., Liu Z., Particle Trapping and Transport Achieved *via* an Adjustable Acoustic Field above a Phononic Crystal Plate, *Journal of Applied Physics*, **119**: 214502 (2016).

[22] Guo J., Kang Y., Ai Y., Radiation Dominated Acoustophoresis Driven by Surface Acoustic Waves, *Journal of Colloid and Interface Science*, **455**: 203–211 (2015).

[23] Ma, D.J. Collins, Y. Ai, Single-Actuator Bandpass Microparticle Filtration *via* Traveling Surface Acoustic Waves, *Colloid and Interface Science Communications*, **16**: 6–9 (2017).

[24] Ren L., Chen Y., Li P., Huang P.H., A High-Throughput Acoustic Cell Sorter, *Lab. Chip.*, **15**: 3870–3879 (2015).

[25] Li S., Ding X., Guo F., Chen Y., Lapsley M.I., Lin S.-C. S., Wang L., McCoy J.P., Cameron C.E., Huang T.J., An On-Chip, Multichannel Droplet Sorter Using Standing Surface Acoustic Waves, *Analytical Chemistry*, 85: 5468–5474 (2013).

[26] Voiculescu I., Nordin A.N., Acoustic Wave Based MEMS Devices for Biosensing Aplications, *Biosensors and Bioelectronics*, **33**: 1-9 (2012).

[27] Lenshof A., Magnusson C., Laurell T., Acoustofluidics 8: Applications of Acoustophoresis in Continuous Flow Microsystems, *Lab on a Chip*, **12**: 1210-1223 (2012).

[28] Muller P.B., Barnkob R., Jense M.J.H., Bruus H., A Numerical Study of Microparticle Acoustophoresis Driven by Acoustic Radiation Forces and Streaming-induced Drag Forces, *Lab. on a Chip.*, **12**: 4617-4627 (2012).

[29] Shamloo A., Boodaghi M., Design and Simulation of a Microfluidic Device for Acoustic Cell Separation, *Ultrasonics*, **84**: 234–243 (2018).

[30] Lei J., Cheng F., Li K., Guo Z., Numerical Simulation of Continuous Separation of Microparticles in Two-Stage Acousto-microfluidic Systems, *Applied Mathematical Modeling*, **S0307-904X**: 30124-4 (2020).

[31] Bruus, H., "Theoretical Microfluidics," Oxford University Press, Oxford, 2008.

[32] Trujillo F.J., Juliano P., Barbosa-Cảnovas G., Knoerzer K., Separation of Suspensions and Emulsions via Ultrasonic Standing Waves–A Review, *Ultrasonics Sonochemistry*, **21**: 2151–2164 (2014).

[33] Trujillo F.J., Eberhardt S., Möller D., Dual J., Knoerzer K., Multiphysics Modelling of the Separation of Suspended Particles *via* Frequency Ramping of Ultrasonic Standing Waves, *Ultrasonics Sonochemistry*, **20**: 655–666 (2013).

[34] Franke T., Hoppe R.H.W., Linsenmann C., Schmid L., Wixforth A., "Optimal Control of Surface Acoustic Wave Actuated Sorting of Biological Cells," University of Houston, Department of Mathematics, Numerical Analysis and Scientific Computing, USA, 505-519 (2013).

[35] Jo M.C., Guldiken R., Active Density-based Separation Using Standing Surface Acoustic Waves, *Sensors and Actuators A*, **187**: 22–28 (2012).

[36] Destgeer G., Jung J.H., Park J., Ahmed H., Park K., Ahmed R., Sung H.J., Acoustic Impedance-Based Manipulation of Elastic Microspheres Using Travelling Surface Acoustic Waves, *The Royal Society of Chemistry*, **7**: 22524-22530 (2017).

[37] Petersson F., Nilsson A., Holm C., Jönsson H., Laurell T., Separation of Lipids from Blood Utilizing Ultrasonic Standing Waves in Microfluidic Channels, *The Royal Society of Chemistry*, **129**: 938-943 (2004).

[38] Taatizadeh E., Dalili A., Rellstab-Sánchez P.I., Tahmooressi H., Ravishankara A., Tasnim N., Hoorfar M., Micron-sized Particle Separation with Standing Surface Acoustic Wave—Experimental and Numerical Approaches, *Ultrasonics Sonochemistry*, **76**: 105651 (2021).